

Resonance shifts and spill-out effects in self-consistent hydrodynamic nanoplasmonics

Giuseppe Toscano,^{*,†,‡} Jakob Straubel,[‡] Alexander Kwiatkowski,[‡] Carsten
Rockstuhl,^{‡,¶} Ferdinand Evers,^{§,¶} Hongxing Xu,^{||,†} N. Asger Mortensen,^{⊥,#} and
Martijn Wubs^{⊥,#}

*Center for Nanoscience and Nanotechnology, School of Physics and Technology, and
Institute for Advanced Studies, Wuhan University, Wuhan 430072, China, Institut für
Theoretische Festkörperphysik, Karlsruhe Institute of Technology (KIT), D-76131
Karlsruhe, Germany, Institute of Nanotechnology, Karlsruhe Institute of Technology
(KIT), Hermann-von-Helmholtz-Platz 1, D-76021 Eggenstein-Leopoldshafen, Germany,
Institut I - Theoretische Physik, Universität Regensburg, Universitätsstraße 31, D-93053
Regensburg, Germany, Beijing National Laboratory for Condensed Matter Physics and
Institute of Physics, Chinese Academy of Sciences, Beijing 100190, China, DTU Fotonik,
Department of Photonics Engineering, Technical University of Denmark, DK-2800 Kgs.
Lyngby, Denmark, and Center for Nanostructured Graphene (CNG) , Technical University
of Denmark, DK-2800 Kgs. Lyngby, Denmark*

E-mail: giuseppe.toscano@kit.edu

Abstract

The standard hydrodynamic Drude model with hard-wall boundary conditions can give accurate quantitative predictions for the optical response of noble-metal nanoparticles. However, it is less accurate for other metallic nanosystems, where surface effects due to electron density spill-out in free space cannot be neglected. Here we address the fundamental question whether the description of surface effects in plasmonics necessarily requires a fully quantum-mechanical approach, such as time-dependent density-functional theory (TD-DFT), that goes beyond an effective Drude-type model. We present a more general formulation of the hydrodynamic model for the inhomogeneous electron gas, which additionally includes gradients of the electron density in the energy functional. In doing so, we arrive at a Self-Consistent Hydrodynamic Model (SC-HDM), where spill-out emerges naturally. We find a redshift for the optical response of Na nanowires, and a blueshift for Ag nanowires, which are both in quantitative agreement with experiments and more advanced quantum methods. The SC-HDM gives accurate results with modest computational effort, and can be applied to arbitrary nanoplasmonic systems of much larger sizes than accessible with TD-DFT methods. Moreover, while the latter typically neglect retardation effects due to time-varying magnetic fields, our SC-HDM takes retardation fully into account.

*To whom correspondence should be addressed

[†]Center for Nanoscience and Nanotechnology, School of Physics and Technology, and Institute for Advanced Studies, Wuhan University, Wuhan 430072, China

[‡]Institut für Theoretische Festkörperphysik, Karlsruhe Institute of Technology (KIT), D-76131 Karlsruhe, Germany

[¶]Institute of Nanotechnology, Karlsruhe Institute of Technology (KIT), Hermann-von-Helmholtz-Platz 1, D-76021 Eggenstein-Leopoldshafen, Germany

[§]Institut I - Theoretische Physik, Universität Regensburg, Universitätsstraße 31, D-93053 Regensburg, Germany

^{||}Beijing National Laboratory for Condensed Matter Physics and Institute of Physics, Chinese Academy of Sciences, Beijing 100190, China

[⊥]DTU Fotonik, Department of Photonics Engineering, Technical University of Denmark, DK-2800 Kgs. Lyngby, Denmark

[#]Center for Nanostructured Graphene (CNG), Technical University of Denmark, DK-2800 Kgs. Lyngby, Denmark

Keywords

Surface plasmons, Density Functional Theory, Scattering, Metal Optics, Quantum Plasmonics.

Introduction

Many recent experiments on dimers and other structures in nanoplasmonics have revealed phenomena beyond classical electrodynamics, but their nature is not always clear and often debated. To explain these new phenomena, a unified theory would be highly desirable that includes nonlocal response, electronic spill-out, as well as retardation. And ideally such a theory would lead to an efficient concomitant computational method. To this end, one could try to generalize standard density-functional theory to include retardation, or to generalize standard hydrodynamic theory so as to include free-electron spill-out at metal-dielectric interfaces. In this Letter we present the latter, both the generalized hydrodynamic theory and its efficient numerical implementation.

The hydrodynamic Drude model of the electron gas is one of the most commonly used methods for the computational study of plasmonic nanostructures beyond classical electrodynamics.¹ This model has been used in recent years to determine the optical response of coupled nanoparticles,^{2–10} the limitations on field enhancement in subwavelength regions,^{11,12} the nanofocusing performances of plasmon tips,¹³ and the fundamental limitations of Purcell factors in plasmonic waveguides.¹⁴ The most important feature of this model is its ability to describe the plasmonic response of noble metals nanoparticles at size regimes at which the classical Drude metal is no longer valid, with a high accuracy and a low computational effort. This is obtained by including the Thomas–Fermi pressure in the equation of motion of the electron gas¹ that takes into account the fermion statistics of the electrons. The hydrodynamic Drude model provides accurate predictions of the spectral positions of the surface plasmon resonances (SPR) for noble-metal dimers, and for single particles it

mimics the SPR blueshift that grows as the particle size decreases.

In line with the local-response Drude model, the standard implementation of the hydrodynamic Drude model considers the so-called *hard-wall boundary condition*, that implies that the electrons are strictly confined in the metallic structure, with a uniform equilibrium density and without spill-out in free space.¹ This approximation is more accurate for noble metals, that show a high work function,¹⁵ than for alkali metals,^{16–19} where the electron density spill-out in free-space characterizes the plasmonic response. This is a well-known limitation of the hydrodynamic Drude model,²⁰ and many attempts have been made to overcome it, thus far with limited success.

In a pioneering attempt, Schwartz and Schaich²¹ proposed to relax the hard-wall constraint by introducing equilibrium electron-density distributions obtained with different methods in the hydrodynamic equations. They found that continuous surface densities lead to the proliferation of spurious surface multipole modes, qualitatively disagreeing with experimental results, which lead them to conclude that the HDM approach to surface effects is subject to a considerable uncertainty. This was disputed by Zaremba and Tso,²² who pointed out that the equilibrium density of the electrons in a metal cannot be chosen arbitrarily, but it must be calculated self-consistently within the hydrodynamic theory itself.

In this Letter we introduce a novel self-consistent hydrodynamic theory for the inhomogeneous electron gas. Hard-wall or other additional boundary conditions are no longer needed and electronic spill-out emerges naturally. We apply this method to the study of the optical response of alkali (Na) and noble-metal (Ag) nanowires, because sodium nanowires were recently used as an example to illustrate the lack of accuracy of standard hydrodynamic theory.^{18,19} By contrast, without any fitting and without heavy computations we obtain with our self-consistent hydrodynamic method accurate agreement both with experiments and with more advanced theories. This illustrates the promising use of our self-consistent hydrodynamic method in nanoplasmonics, where efficient methods that take into account retardation, nonlocal response, as well as spill-out are highly demanded but scarce.

Hydrodynamic equations

We first briefly recall how in general hydrodynamic equations are derived in terms of functional derivatives of the internal energy of an electron plasma, before specifying our choice for the internal energy. The Bloch hydrodynamic Hamiltonian for the inhomogeneous electron gas²³ reads:

$$H[n(\mathbf{r}, t), \mathbf{p}(\mathbf{r}, t)] = G[n(\mathbf{r}, t)] + \int \frac{(\mathbf{p}(\mathbf{r}, t) - e\mathbf{A}(\mathbf{r}, t))^2}{2m} n(\mathbf{r}, t) d\mathbf{r} + e \int \phi(\mathbf{r}, t) n(\mathbf{r}, t) d\mathbf{r} + e \int V_{\text{back}}(\mathbf{r}) n(\mathbf{r}, t) d\mathbf{r}, \quad (1)$$

where $n(\mathbf{r}, t)$ is the electron density and $\mathbf{p}(\mathbf{r}, t) = m\mathbf{v}(\mathbf{r}, t) + e\mathbf{A}(\mathbf{r}, t)$ its conjugate momentum, with e being the electron charge and m the electron mass. The electrons are coupled to the electromagnetic field associated with the retarded potentials $\phi(\mathbf{r}, t)$ and $\mathbf{A}(\mathbf{r}, t)$, i.e. $\mathbf{E}(\mathbf{r}, t) = -\nabla\phi(\mathbf{r}, t) - \frac{\partial\mathbf{A}(\mathbf{r}, t)}{\partial t}$ and $\mathbf{B}(\mathbf{r}, t) = \nabla \times \mathbf{A}(\mathbf{r}, t)$. The electrostatic potential $V_{\text{back}}(\mathbf{r})$ is a confining background potential, that is associated with the electrostatic field generated by the positive ions in a metal, i.e. $\nabla^2 V_{\text{back}}(\mathbf{r}) = -\rho^+(\mathbf{r})/\varepsilon_0$, where $\rho^+(\mathbf{r})$ is the positive charge density of the metal ions. The term $G[n(\mathbf{r}, t)]$ is the internal energy of the electron gas, which is assumed to be a functional of the electron density. Its functional form is not known *a priori* and we will specify and motivate our particular choice later. The equations of motion can be obtained from eq 1 by means of the methods of the Hamiltonian formulation of fluid dynamics^{24–26} (see Supplemental Material).

The force balance on a fluid element is stated by the Euler equation [and in the following we will for simplicity suppress the (\mathbf{r}, t) dependence]

$$mn\left(\frac{\partial\mathbf{v}}{\partial t} + \mathbf{v} \cdot \nabla\mathbf{v}\right) = -n\nabla\frac{\delta G}{\delta n} + ne(\mathbf{E} + \mathbf{v} \times \mathbf{B}), \quad (2)$$

where the density n satisfies the charge continuity equation

$$\frac{\partial n}{\partial t} = -\nabla \cdot (n\mathbf{v}). \quad (3)$$

We focus on the linear response of the electron gas described by eq 1, so we solve eqs 2 and 3 for small perturbations of the electron density $n_1(\mathbf{r}, t)$ around the equilibrium density $n_0(\mathbf{r})$, i.e. $n(\mathbf{r}, t) = n_0(\mathbf{r}) + n_1(\mathbf{r}, t)$.²⁷ It can be shown (see Supplemental Material) that $n_0(\mathbf{r})$ satisfies

$$\left(\frac{\delta G}{\delta n}\right)_0 + e(\phi_0 + V_{\text{back}}) = \mu, \quad (4)$$

where ϕ_0 is the potential associated with the electrostatic field \mathbf{E}_0 generated by the equilibrium charge density $\rho_0 = en_0$. Thus ϕ_0 and ρ_0 are related by Poisson's equation $\nabla^2 \phi_0(\mathbf{r}) = -\rho_0(\mathbf{r})/\varepsilon_0$. The quantity $\left(\frac{\delta G}{\delta n}\right)_0$ is the functional derivative evaluated at the equilibrium density n_0 , and μ represents the (constant) chemical potential of the electron gas. Equation 4 is quite general and also appears in standard density functional theory.^{28,29}

It is useful to write the linearized versions of both the force-balance eq 2 and the charge continuity eq 3 in terms of the electric-charge density perturbation $\rho_1 = en_1$, and the first-order electric current-density vector $\mathbf{J}_1 = en_0\mathbf{v}_1 \equiv \rho_0\mathbf{v}_1$. The linearized Euler equation for the current-density vector \mathbf{J}_1 reads

$$\frac{\partial \mathbf{J}_1}{\partial t} = -\frac{\rho_0}{m}\nabla\left(\frac{\delta G}{\delta n}\right)_1 + \omega_p^2\varepsilon_0\mathbf{E}_1, \quad (5)$$

while the linearized continuity equation becomes

$$\nabla \cdot \mathbf{J}_1 = -\frac{\partial \rho_1}{\partial t}. \quad (6)$$

The quantity $\left(\frac{\delta G}{\delta n}\right)_1$ in eq 5 is given by $\left.\frac{\delta G}{\delta n}\right|_{n_0+n_1} - \left.\frac{\delta G}{\delta n}\right|_{n_0}$, and $\omega_p = [e^2 n_0 / (m\varepsilon_0)]^{1/2}$ is the common plasma frequency of the electron gas.

The vector fields \mathbf{E}_1 and \mathbf{J}_1 satisfy Maxwell's wave equation

$$\nabla \times \nabla \times \mathbf{E}_1 + \frac{1}{c^2} \frac{\partial^2 \mathbf{E}_1}{\partial t^2} = -\mu_0 \frac{\partial \mathbf{J}_1}{\partial t}. \quad (7)$$

The linear system given by eqs 5, 6, and 7 is closed, and can be solved once the equilibrium density $\rho_0(\mathbf{r})$ has been calculated by means of eq 4 (see Supplemental Material). It is important to notice that retardation effects due to time-varying magnetic fields are included in the system above, so that both longitudinal and transverse solutions are possible. This is an important difference with state-of-the-art TD-DFT methods, that only solve for longitudinal currents and electric fields.³⁰

The linearization procedure of the hydrodynamic equations that we have outlined so far is logically consistent, since no external assumptions on the quantities involved are required. In particular, rather than a postulated function, the static electron density $n_0(\mathbf{r})$ is a solution of eq. 4. We call this method “Self-Consistent Hydrodynamic Model” (SC-HDM), in order to distinguish it from other implementations of the hydrodynamic model that employ an arbitrarily chosen equilibrium charge density. And for our choice of the energy functionals as detailed below, we will be able to describe electronic spill-out, i.e. a non-vanishing $n(\mathbf{r})$ also outside the metal.

Hydrodynamic Drude model

The hydrodynamic Drude model commonly used in nanoplasmonics can be presented in terms of the general hydrodynamic theory developed above. We recall here the equation of motion for this model, that in time domain reads¹

$$\frac{\partial \mathbf{J}_1}{\partial t} = -\beta^2 \nabla \rho_1 + \omega_p^2 \varepsilon_0 \mathbf{E}_1, \quad (8)$$

where β is called *hydrodynamic parameter*, defined as $\beta = \sqrt{3/5} v_F$, and v_F is the Fermi velocity, $v_F = \frac{\hbar}{m} (3\pi^2)^{1/3} n_0^{1/3}$. In the usual implementations of the hydrodynamic Drude

model, a uniform equilibrium electron density $n_0(\mathbf{r}) = n_0$ is assumed, and the electron density spill-out in free space is neglected. This leads to the *hard-wall boundary condition*, stating that the current density vector \mathbf{J}_1 has a vanishing normal component at the surface of the metallic nanostructures. For this reason, in the next sections we will refer to this model as “Hard-Wall Hydrodynamic Model” (HW-HDM).

It can be readily shown that eq 8 can be derived from eq 5, if we consider $n_0(\mathbf{r}) = n_0$ inside the metal, and approximate the internal energy $G[n]$ by means of the Thomas–Fermi kinetic energy functional multiplied by a constant parameter $\alpha = 9/5$ that account for the high frequency corrections³¹ (see below the discussion about the choice of the energy functionals). Moreover, it is possible to prove that a uniform equilibrium electron density is a solution of eq 4, thus the hydrodynamic Drude model is a special case of the SC-HDM (see Supplemental Material).

Finally, we would like to mention that if the hydrodynamic parameter β vanishes, eq 8 reduces to the Drude equation of motion for the free-electron gas. We call this well-known model “Local Response Approximation” (LRA), since it neglects nonlocal electromagnetic effects associated with the derivative of the charge density ρ_1 in the equation of motion.

Including density gradients in the energy functional

After obtaining the closed system of linearized hydrodynamic equations, we now specify and motivate the form of the energy functional that features in them. The internal energy functional $G[n(\mathbf{r}, t)]$ in eq 1 is given, in general, by the sum of a kinetic energy functional $T[n(\mathbf{r}, t)]$ and an exchange-correlation (XC) energy functional $F_{\text{xc}}[n(\mathbf{r}, t)]$:²⁹

$$G[n(\mathbf{r}, t)] = T[n(\mathbf{r}, t)] + F_{\text{xc}}[n(\mathbf{r}, t)].$$

In TD-DFT, the kinetic-energy term $T[n(\mathbf{r}, t)]$ is calculated by means of the Kohn–Sham equations, a task that is computationally demanding for particles consisting of much more

than 10^3 electrons, in other words for most experiments in nanoplasmonics. The main goal of our SC-HD model is therefore to provide an alternative computational tool for particles and structures of larger sizes and lower symmetry than TD-DFT currently can handle. We do this by means of an orbital-free approach.^{32–35} Below we discuss the kinetic- and XC-energy functionals separately.

We approximate the kinetic-energy functional by the sum of the Thomas–Fermi functional and the von Weizsäcker functional,³⁶

$$T_{\text{TFW}}[n] = T_{\text{TF}}[n] + T_{\text{W}}[n] = \frac{3}{10} \frac{\hbar^2}{m} (3\pi^2)^{2/3} \int n^{5/3}(\mathbf{r}, t) d\mathbf{r} + \frac{1}{72} \frac{\hbar^2}{m} \int \frac{|\nabla n(\mathbf{r}, t)|^2}{n(\mathbf{r}, t)} d\mathbf{r}. \quad (9)$$

Here the last term is the von Weizsäcker functional, which is also called the “second-order gradient correction” to the Thomas–Fermi kinetic functional.²⁸ Such a gradient correction can become important in space regions where $n_0(\mathbf{r})$ shows strong variations, for example in the vicinity of metal surfaces as we shall see below, and especially when describing molecules.²⁸ Our choice is motivated by the fact that the T_{TFW} functional is known to provide reliable descriptions of surface effects in metals, and it has been extensively employed in solid-state physics to calculate the work functions and surface potentials of various metals.^{37–41} Although adding the functional T_{TFW} will significantly improve the accuracy of hydrodynamic calculations, it will not reconstruct the wave nature of the electrons, inherent e.g. in the Friedel oscillations into the metal bulk, which require the full Kohn–Sham calculations with XC functionals.⁴²

In nanoplasmonics only the Thomas–Fermi functional was used until now,^{2–14} while to our knowledge the second-order gradient correction has thus far been neglected. Below we will give an example where calculations of optical properties based on only the Thomas–Fermi functional disagree with experiment, while agreement is found when including the von Weizsäcker functional, in combination with the XC functionals as discussed below.

An exact expression for the XC functional is not known in general,⁴³ and it is not easy to

calculate it numerically either, so an approximation of the $F_{xc}[n(\mathbf{r}, t)]$ is commonly employed, for example for doing TD-DFT calculations. The most familiar one is the local-density approximation (LDA), where the name implies that no density gradients are considered in the construction of the functional. Just like for the kinetic functional, gradient corrections to the XC functional may nonetheless become significant for inhomogeneous systems. This calls for nonlocal density approximations (NLDA) beyond LDA, in order to correct for long-range effects arising for strong density variations.

On a par with our treatment of the kinetic functional, we will also include density gradients in the XC-functional that enters our hydrodynamic equations. In particular, we include the Gunnarson and Lundqvist (GL) LDA XC functional,⁴⁴ that has been used both for Na^{19,45} and Ag.⁴⁶ Additionally, we include a non-local correction (NLDA) for long-range effects, namely the van Leeuwen and Baerends potential (LB94),⁴⁷ which has already been used for Ag and Au plasmonic nanostructures.^{48,49} Incidentally, when leaving out the NLDA exchange term to the functional, we found non-physical solutions with density tails propagating in the free-space region.

Hereby we have specified and motivated the total energy functional that we will employ in our hydrodynamic theory. The inclusion of the density-gradient terms will make the crucial difference with state-of-the-art hydrodynamic theory used in plasmonics. We will soon show predictions that agree well both with experiments and with more advanced theory. Yet we want to point up that we do not claim to have identified the unique and only functionals. For example, more refined gradient corrections to the kinetic energy functionals have been proposed in the literature,^{50–52} and they might be needed in order to approximate the DFT results for specific cases.

Implementation of the SC-HD model

We implemented the SC-HD model with the finite-element method in the commercially available software COMSOL Multiphysics 4.2a. Equation 4 is nonlinear in the electron

density, and it can be easily implemented when the ionic background of the metallic system is specified. We employ the jellium model for the ions, a standard approximation that is also successfully adopted in state-of-the-art TD-DFT calculations.^{18,19,53}

The linear differential system given by eqs 5 and 7 was transformed to the frequency domain. We then solved for the induced charge density ρ_1 instead of the induced current-density vector \mathbf{J}_1 . This is numerically advantageous, since it allows to solve for only one variable (ρ_1) instead of the three components of \mathbf{J}_1 . The full implementation procedure is described in detail in the Supplemental Material.

Sodium Nanowires - Optical response

We apply our formalism to derive the optical response of a Na cylindrical nanowire of radius $R = 2$ nm. In the first step of our analysis, we calculate the equilibrium electron density n_0 of the Na nanowire by means of eq 4. The positive background density of the jellium is given by the ion density of Na, i.e. $n^+ = 2.5173 \times 10^{28} \text{ m}^{-3}$. The result is shown in fig 1b (dashed line). Besides the charge spill-out into free space, n_0 also exhibits an oscillation within the metal. This is somewhat reminiscent of Friedel oscillations, whereas true Friedel oscillations at wavelength $\lambda_F/2$ with the correct envelope require solving the full Kohn–Sham equation with suitable XC functionals.

To determine the optical response of the system, we irradiate the nanowire with an in-plane polarized plane wave of amplitude $E_0 = 1 \text{ V/m}$, as in ref 4. All the perturbed quantities are calculated by means of the equation of motion eq 5, where a damping factor γ is introduced to take into account the electron-phonon interaction, dissipation due to the electron-hole continuum, impurity scattering, etc. We choose the value $\hbar\gamma = 0.17 \text{ eV}$ from ref 54. Interband effects are not included, since for Na their effects in the visible range are negligible.⁵⁵

The optical quantity that we consider is the absorption cross section per unit length σ_{abs} ,

defined as $\sigma_{\text{abs}} = \frac{P_{\text{abs}}}{2RI_0}$, where $I_0 = \varepsilon_0 c E_0^2 / 2$ is the power density of the perturbing field. We compare the prediction by the SC-HD model with both the HW-HDM and with the usual local-response approximation (LRA). The hydrodynamic parameter β for the HW-HDM is $\beta = \sqrt{3/5} v_F$, where the Fermi velocity for Na is $v_F = 0.82 \times 10^6$ m/s.

The results are shown in Figure 1a. The main SPR within the LRA occurs at $\hbar\omega_{\text{res}} = 4.158$ eV. This resonance is *blueshifted* by 0.139 eV to become $\hbar\omega_{\text{res}} = 4.297$ eV in the HW-HDM. In stark contrast, for the SC-HD model the resonance appears at $\hbar\omega_{\text{res}} = 4.017$ eV, in other words *redshifted* by 0.141 eV with respect to the LRA.

Apart from their different peak positions, the three SPRs in the absorption cross section in Figure 1a also exhibit different peak heights in the three models. An intuitive explanation for this behavior could be provided on the basis of the different geometrical cross sections in the three models: in the SC-HDM the electrons spill out from the surface of the nanowire, so the structure appears bigger than in the LRA. In contrast, the free electrons are pushed inwards into the metal in the HW-HD model, so this structure looks smaller than in the LRA.

The redshift of the surface-plasmon resonance in Na is linked to the electron spill-out in free space, or more precisely, to the fact that the centroid of the induced charge density ρ_1 associated with the SPR is placed outside the jellium edge.^{17,19,56} Our self-consistent calculations correctly reproduce this feature of ρ_1 at the SPR peak, as it is shown in Figure 1b (filled line). This plot highlights a peak of ρ_1 in the free-space region and a dip in the internal region where the equilibrium density takes its maximal value. We normalized the induced charge density ρ_1 with respect to E_0 , since in the considered linear-response regime the induced charge density is linearly proportional to the amplitude of the applied field.

To further confirm the validity of our method, we would like to stress that the spectral position $\hbar\omega_{\text{res}} = 4.017$ eV of the SPR that we obtained within our semiclassical hydrodynamic theory, is in good agreement with the values obtained with TD-DFT methodologies for similar systems.^{18,19} A perfect agreement is not achievable because of the different ap-

proximations that are intrinsic to each specific method.

The absorption cross section spectrum in Figure 1a shows another resonance peak at $\hbar\omega_{\text{res}} = 4.918 \text{ eV}$. This resonance is known in the literature as “multipole surface plasmon” or “Bennett resonance”, first predicted by Bennett in 1970.⁵⁷ The charge distribution ρ_1 associated with this resonance is characterized by the fact that its integral along a direction orthogonal to the surface vanishes identically⁵⁸ (see Figure 3). The Bennett resonance is not observable in the LRA and HW-HD models in Figure 1, since it is an effect of the non-uniform charge density in the metal and the electron spill-out in vacuum.⁵⁷ We would like to point out that also in this case the spectral position of the Bennett resonance that we find is in the same range of the results obtained with other methods.^{18,19,56,57,59}

Figure 1c shows again an equilibrium electron density n_0 and an induced charge density ρ_1 , but now for the HW-HD model. Consistent with the hard-wall assumption, all charges in Figure 1c are indeed localized inside the metal. The equilibrium density n_0 is constant and equal to the local-response value for bulk Na, whereas the induced density ρ_1 can be seen to decrease monotonically away from the surface, where in local response (not shown) all induced charge would reside in a delta-function distribution on the interface. Finally, a comparison of Figures 1b,c nicely illustrates that the non-monotonous equilibrium and induced charge densities in the metal region and the spill-out in the air region are a consequence of taking density gradients into account in the energy functional of our self-consistent hydrodynamic theory.

Silver Nanowires - Optical Response

We will now compare the optical response of Ag nanowires with that of Na nanowires as discussed above. The aim is to show that our self-consistent HD theory for both types of metals agrees with experiment and with TD-DFT calculations.

The free-electron gas in Ag consists of electrons in the 5s-band. Analogous to the case

of Na that we discussed above, their spatial equilibrium distribution n_0 can be calculated within the jellium approximation for the positive-charge background. Such calculations of n_0 have already been done for noble metals, in DFT calculations for example.^{46,53,56}

However, unlike for Na, for Ag the interband transitions from the filled 4d-band to the 5s-band near to the Fermi level often cannot be neglected in the optical response, so that Ag cannot be described as a pure Drude metal at optical frequencies. Because of this well-known fact, we will take interband transitions into account in our SC-HD model for Ag. In principle, a full-electron calculation could be used to account for interband transitions. However, this is computationally very demanding and beyond the aims and scope of our hydrodynamic approach. For this reason, we follow the prescription proposed by Liebsch,⁵⁶ treating the 4d-core electrons as an effective polarizable medium that contributes to the optical response by means of an interband permittivity $\varepsilon_{\text{inter}}$. This medium is assumed to extend up to the first plane of nuclei. In the jellium model, the distance d between the edge of the positive background and the first plane of nuclei amounts to half a lattice spacing, and this parameter can be obtained from experimental data on the specific metallic system. For example, in the case of the Ag (111), (001), and (110) faces, d is equal to 1.18, 1.02, and 0.72 Å, respectively.⁵⁶

For a good comparison, we again study nanowires of radius $R = 2$ nm that are irradiated by a plane wave with in-plane polarization and amplitude $E_0 = 1$ V/m. For Ag the ion density is $n^+ = 5.8564 \times 10^{28} \text{ m}^{-3}$, corresponding to a plasma frequency $\hbar\omega_p = 9.01$ eV. For the hydrodynamic parameter β for Ag we employ $v_F = 1.39 \times 10^6$ m/s. The interband permittivity $\varepsilon_{\text{inter}}$ for Ag is obtained from ref 60. In the SC-HD model we fix (rather than fit) the distance parameter at $d = 1$ Å, which is of the order of the aforementioned distances between the first plane of nuclei and the edge of the jellium background.⁵⁶ By contrast, for the HW-HD model we take d to vanish, because the free electrons do not spill into free space in this case.¹¹

Figure 2a shows absorption cross sections for the Ag nanowire, computed for the same

three models as for the Na nanowire in Figure 1. But this time for Ag both the HW- and the SC-HD models exhibit blueshifts with respect to the local-response surface-plasmon resonance at $\hbar\omega_{\text{res}} = 3.594 \text{ eV}$. In particular, in the HW-HD model the resonance occurs at $\hbar\omega_{\text{res}} = 3.664 \text{ eV}$ (i.e. blueshifted by 0.0697 eV), while for the SC-HD model the resonance is at $\hbar\omega_{\text{res}} = 3.653 \text{ eV}$ (a blueshift of 0.0592 eV). As for Na, the difference in the peak values of the absorption cross section can be intuitively explained as a fingerprint of the distinct geometrical cross sections of the scatterers in the three models.

While the blueshift in the HW-HD model is due to the ‘spill-in’ of the electron density inside the metal, the blueshift in the SC-HD model is a more complicated affair, related to the interplay between the 4d-band and 5s-band electrons at the metal-air interface: the induced charge density that contributes to the SPR oscillates at the unscreened plasma frequency in the vacuum region ($\omega_{\text{res}} = \omega_{\text{p}}/\sqrt{2}$), and it oscillates at the screened plasma frequency $\omega_{\text{res}} = \omega_{\text{p}}/\sqrt{1 + \text{Re}(\varepsilon_{\text{inter}})}$ inside the metal. This complex mechanism leads to a net increase of the resonance frequency for Ag nanowires.⁵⁶ Our important point here is that the SC-HD model is the first semiclassical model to account for this mechanism.

Figure 2b shows the equilibrium electron density n_0 for Ag nanowires, exhibiting both the charge spill-out effect and an onset of Friedel oscillations, quite analogous to the case of Na. The induced charge density ρ_1 is also shown, and although for Ag it is screened by the polarization effects of the effective medium due to interband transitions, at least up to a distance d away from the jellium interface, we again see an oscillation in the internal region, and a peak followed by decay in the free-space region.

Figure 2c shows the constant equilibrium electron density n_0 and the induced charge density ρ_1 in the HW-HD model. Both are fully localized inside the nanowire, consistent with the hard-wall assumption. The charge density oscillation is due to the screening effects of the core electrons, in contrast to the monotonous spatial decay of ρ_1 for Na in Figure 1c.

Finally, a comparison of Figures 1a and 2a shows that the absorption cross section of Ag nanowires increases for higher energies, while it drops for Na wires. The difference can be

attributed to interband transitions in Ag that have no counterpart in Na. The interband transitions also prevent the occurrence of a Bennett resonance in Ag nanowires.

Size-dependent frequency shifts

Until now we studied the SPR shifts for both Na and Ag nanowires with a fixed radius of $R = 2$ nm, but to support our interpretations we will now present a systematic study of the dependence of the SPR shifts on the radius of the nanowire. An advantage of our semiclassical SC-HD model is that numerical calculations are feasible also for wires of considerably larger radii. For the HW-HD model in the quasi-static approximation, analytical expressions are known for the size-dependent resonance shift, which in that model is always a blueshift, with a leading $1/R$ scaling.⁶¹ We are now in the position to test whether this scaling behavior is a consequence of the hard-wall approximation, or also occurs in our SC-HD model that allows spill-out of the free electrons.

Figure 4a shows the SPR frequency shift as a function of the inverse radius $1/R$ as computed with the SC-HD model. The red line represents the data for Na. For particles of radius $R < 5$ nm, the resonance frequency varies linearly with $1/R$, with a negative slope of -0.2 eV/nm⁻¹, in other words the SPR frequencies *redshift* when the particle size is decreased. This finding based on our SC-HD model agrees with the numerical results obtained by Li *et al.*,⁶² who also predict the $1/R$ scaling by using TD- DFT methods. The blue line in Figure 4a shows the R -dependent frequency shift for Ag. This time the resonance frequency increases linearly with $1/R$ for wire radii $R < 8$ nm, with slope 0.12 eV/nm⁻¹. Thus our SC-HD model predicts that the SPR frequencies for Ag *blueshift* when decreasing the particle size, in agreement with the $1/R$ scaling observed experimentally by Charlé *et al.*⁶³ So from Figure 4a we can now appreciate that the $1/R$ scaling is not a consequence of the hard-wall approximation, since it is now also found in the SC-HD model that includes electron spill-out. Our major result is of course our hydrodynamic (SC-HD) prediction of

the redshift for Na nanowires in Figure 4a, where the HW-HD model incorrectly predicts a blueshift^{18,19} (not shown here).

It is important to notice that Figure 4a shows a substantial deviation from the $1/R$ dependence for Na already starting for $R > 5$ nm, which we attribute to retardation. A similar but smaller deviation from the $1/R$ scaling for Ag can also be observed in Figure 4, but its onset occurs for slightly larger radii, namely for $R > 8$ nm. To substantiate our claim that the deviations from the $1/R$ scaling in our SC-HD model are due to retardation, we also present LRA calculations of the dependence of the SPR peak value for σ_{abs} on the particle radius. In the quasi-static regime this peak value follows a power-law distribution,⁶⁴ $\sigma_{\text{abs}} \propto R^k$, which on a log-log plot as in the inset of Figure 4 would give a straight line of slope k . The clear deviation from such power-law behavior already for Na wires of radii smaller than 10 nm illustrates that the effects of the retardation become important for rather thin plasmonic nanowires also in the LRA. Wire radii of at least tens of nanometers are more typical in nanoplasmonic experiments. The main panel in Figure 4 thus also nicely illustrates that the SC-HD model combines two important features: first, it describes free-electron nonlocal response and spill-out, leading to $1/R$ size-dependent blueshifts for some metals and redshifts for others; second, it takes retardation fully into account, which for larger wires redshifts surface-plasmon resonances away from their quasi-static values.

Finally, we consider the Bennett resonance frequency shift as a function of the inverse radius $1/R$ as computed with the SC-HD model (Figure 4b). For particles of radius $R < 4$ nm, the resonance frequency varies linearly with $1/R$, with a positive slope of 0.14 eV/nm^{-1} , i.e. the Bennett resonance frequencies *blueshift* when the particle size is decreased.

Conclusion

In conclusion, we have shown that the Self-Consistent Hydrodynamic Model is able to describe not only nonlocal response but also electronic spill-out of both noble (Ag) and simple

(Na) metals. Both the signs and the values of the resonance shifts obtained with this method agree with experimental results and predictions obtained with ab-initio methods. The SPR blueshift for Ag versus the redshift for Na are only a consequence of different well-known parameters: Drude parameters, Fermi velocities, interband permittivities $\varepsilon(\omega)$, and the spacing d between the jellium edge and the first plane of nuclei.

Moreover, Bennett resonances could be identified here for the first time in a semiclassical model. We also systematically studied the size dependence of the Bennett resonance, which we believe has not been done before by other methods. We found that the Bennett resonance frequencies *blueshift* when the particle size is decreased.

The SC-HDM was obtained by extending state-of-the-art hydrodynamic models considered in nanoplasmonic research to consistently include gradients of the density into the energy functional that governs the semiclassical dynamics. Thus the inability of previous hydrodynamic models to find redshifts of surface plasmon resonances for nanoparticles consisting of simple metals cannot be held against hydrodynamic models as such. Rather, it was a consequence of using too simple energy functionals that neglected terms involving gradients of the electron density, terms which become important near metal-dielectric interfaces, being most pronounced for Na while spectrally of minor importance for Ag and Au nanowires.

Moreover, the SC-HDM model includes the effects of retardation, that are not treated in TD-DFT, unless more complicated schemes are adopted.⁶⁵ It provides a fast, flexible and reliable tool that gives the exciting possibility to treat electronic spill-out and nonlocal response in relatively large-size systems of arbitrary shapes that are of interest in the nanoplasmonic applications. Think for example of large dimers with small gap sizes.

For Ag nanowires we find quite good agreement between plasmonic resonances in the SC-HD model and in the simpler HW-HD model that neglects spill-out, justifying the use of the simpler model when not focusing on spill-out. We maintain that this good agreement for Ag (and the not so good agreement for Na) found here is not fortuitous. Rather, the agreement becomes systematically better for metals with higher work functions.

Our main goal has been to develop a versatile hydrodynamic theory and numerical method that account for both retardation and electronic spill-out, and here we have shown how this can be done. We do not claim that our energy functional is unique, and we stressed that other self-consistent hydrodynamic theories are possible (see Supplementary Material and refs. 32,34). We have not tried to be as accurate as possible by fitting density-functional parameters either to experimentally measured values or to more microscopic calculations. For example, one could add fitting functions to the energy functional, fit them for a simple geometry, and use them for more complex geometries. Indeed there is plenty of room to obtain even better agreement with more advanced theories. But exactly by not doing such fits, the good agreement that we already find here is interesting and promising.

In the future we will employ our SC-HD model to other more complex geometries. While in the present work we have mainly focused on size-dependent frequency shifts, we envisage that in the future this model can be extended to also include size-dependent damping.⁶⁶

Acknowledgement

The authors thank Dr. Shunping Zhang from Wuhan University, Prof. Shiwu Gao from the University of Gothenburg, Prof. Javier Aizpurua from the Donostia International Physics Center (DIPC), as well as Prof. Kristian S. Thygesen, Søren Raza, and Dr. Wei Yan from the Technical University of Denmark for inspiring discussions. The Center for Nanostructured Graphene is sponsored by the Danish National Research Foundation, Project DNRF58. This work was also supported by the Danish Council for Independent Research - Natural Sciences, Project 1323-00087.

References

- (1) Raza, S.; Toscano, G.; Jauho, A.-P.; Wubs, M.; Mortensen, N. A. *Phys. Rev. B* **2011**, *84*, 121412(R).

- (2) McMahon, J. M.; Gray, S. K.; Schatz, G. C. *Phys. Rev. Lett.* **2009**, *103*, 097403.
- (3) David, C.; García de Abajo, F. J. *J. Phys. Chem. C* **2011**, *115*, 19470–19475.
- (4) Toscano, G.; Raza, S.; Jauho, A.-P.; Mortensen, N. A.; Wubs, M. *Opt. Express* **2012**, *20*, 4176 – 4188.
- (5) Dong, T.; Ma, X.; Mittra, R. *Appl. Phys. Lett.* **2012**, *101*, 233111.
- (6) Fernández-Domínguez, A. I.; Wiener, A.; García-Vidal, F. J.; Maier, S. A.; Pendry, J. B. *Phys. Rev. Lett.* **2012**, *108*, 106802.
- (7) Fernández-Domínguez, A. I.; Zhang, P.; Luo, Y.; Maier, S. A.; García-Vidal, F. J.; Pendry, J. B. *Phys. Rev. B* **2012**, *86*, 241110.
- (8) Ciracì, C.; Urzhumov, Y.; Smith, D. R. *J. Opt. Soc. Am. B* **2013**, *30*, 2731–2736.
- (9) Luo, Y.; Fernández-Domínguez, A. I.; Wiener, A.; Maier, S. A.; Pendry, J. B. *Phys. Rev. Lett.* **2013**, *111*, 093901.
- (10) Wiener, A.; Duan, H.; Bosman, M.; Horsfield, A. P.; Pendry, J. B.; Yang, J. K. W.; Maier, S. A.; Fernández-Domínguez, A. I. *ACS Nano* **2013**, *7*, 6287–6296.
- (11) Toscano, G.; Raza, S.; Xiao, S.; Wubs, M.; Jauho, A.-P.; Bozhevolnyi, S. I.; Mortensen, N. A. *Opt. Lett.* **2012**, *37*, 2538–2540.
- (12) Ciracì, C.; Hill, R. T.; Mock, J. J.; Urzhumov, Y.; Fernández-Domínguez, A. I.; Maier, S. A.; Pendry, J. B.; Chilkoti, A.; Smith, D. R. *Science* **2012**, *337*, 1072–1074.
- (13) Wiener, A.; Fernández-Domínguez, A. I.; Horsfield, A. P.; Pendry, J. B.; Maier, S. A. *Nano Lett.* **2012**, *12*, 3308–3314.
- (14) Toscano, G.; Raza, S.; Yan, W.; Jeppesen, C.; Xiao, S.; Wubs, M.; Jauho, A.-P.; Bozhevolnyi, S.; Mortensen, N. A. *Nanophotonics* **2013**, *2*, 161–166.

- (15) Lang, N. D.; Kohn, W. *Phys. Rev. B* **1971**, *3*, 1215–1223.
- (16) Brack, M. *Rev. Mod. Phys.* **1993**, *65*, 677–732.
- (17) Weick, G.; Ingold, G.-L.; Jalabert, R. A.; Weinmann, D. *Phys. Rev. B* **2006**, *74*, 165421.
- (18) Stella, L.; Zhang, P.; García-Vidal, F. J.; Rubio, A.; García-González, P. *J. Phys. Chem. C* **2013**, *117*, 8941–8949.
- (19) Teperik, T. V.; Nordlander, P.; Aizpurua, J.; Borisov, A. G. *Opt. Express* **2013**, *21*, 27306–27325.
- (20) Apell, P.; Ljungbert, Å.; Lundqvist, S. *Physica Scripta* **1984**, *30*, 367–383.
- (21) Schwartz, C.; Schaich, W. L. *Phys. Rev. B* **1982**, *26*, 7008–7011.
- (22) Zaremba, E.; Tso, H. C. *Phys. Rev. B* **1994**, *49*, 8147–8162.
- (23) Bloch, F. *Zeitschrift für Physik* **1933**, *81*, 363–376.
- (24) Morrison, P. J. *Rev. Mod. Phys.* **1998**, *70*, 467–521.
- (25) Morrison, P. J.; Greene, J. M. *Phys. Rev. Lett.* **1980**, *45*, 790–794.
- (26) Morrison, P. J. *Physics of Plasmas* **2005**, *12*, 058102.
- (27) Eguiluz, A.; Quinn, J. J. *Phys. Rev. B* **1976**, *14*, 1347–1361.
- (28) Parr, R. G.; Yang, W. *Density-Functional Theory of Atoms and Molecules*; Oxford University Press, USA, 1994.
- (29) Hohenberg, P.; Kohn, W. *Phys. Rev.* **1964**, *136*, B864–B871.
- (30) Ullrich, C. *Time-Dependent Density-Functional Theory: Concepts and Applications*; Oxford University Press: New York, USA, 2012.
- (31) Halevi, P. *Phys. Rev. B* **1995**, *51*, 7497–7499.

- (32) Vignale, G.; Ullrich, C. A.; Conti, S. *Phys. Rev. Lett.* **1997**, *79*, 4878–4881.
- (33) Banerjee, A.; Harbola, M. K. *J. Chem. Phys.* **2000**, *113*, 5614–5623.
- (34) Giuliani, G. F.; Vignale, G. *Quantum Theory of the Electron Liquid*; Cambridge University Press: Cambridge, UK, 2008.
- (35) Neuhauser, D.; Pistinner, S.; Coomar, A.; Zhang, X.; Lu, G. *J. Chem. Phys.* **2011**, *134*.
- (36) Yang, W. *Phys. Rev. A* **1986**, *34*, 4575–4585.
- (37) Smith, J. R. *Phys. Rev.* **1969**, *181*, 522–529.
- (38) Chizmeshya, A.; Zaremba, E. *Phys. Rev. B* **1988**, *37*, 2805–2811.
- (39) Utreras-Diaz, C. A. *Phys. Rev. B* **1987**, *36*, 1785–1788.
- (40) Tarazona, P.; Chacón, E. *Phys. Rev. B* **1989**, *39*, 10366–10369.
- (41) Snider, D.; Sorbello, R. *Solid State Commun.* **1983**, *47*, 845 – 849.
- (42) Snider, D. R.; Sorbello, R. S. *Phys. Rev. B* **1983**, *28*, 5702–5710.
- (43) Martin, R. M. *Electronic Structure: Basic Theory and Practical Methods*; Cambridge University Press, 2008.
- (44) Gunnarsson, O.; Lundqvist, B. I. *Phys. Rev. B* **1976**, *13*, 4274–4298.
- (45) Ekardt, W. *Phys. Rev. B* **1984**, *29*, 1558–1564.
- (46) Pustovit, V. N.; Shahbazyan, T. V. *Chem. Phys. Lett.* **2006**, *420*, 469 – 473.
- (47) van Leeuwen, R.; Baerends, E. J. *Phys. Rev. A* **1994**, *49*, 2421–2431.
- (48) Guidez, E. B.; Aikens, C. M. *J. Phys. Chem. C* **2013**, *117*, 12325–12336.

- (49) Piccini, G. M.; Havenith, R. W. A.; Broer, R.; Stener, M. *J. Phys. Chem. C* **2013**, *117*, 17196–17204.
- (50) Vitos, L.; Skriver, H. L.; Kollár, J. *Phys. Rev. B* **1998**, *57*, 12611–12615.
- (51) Laricchia, S.; Fabiano, E.; Constantin, L. A.; Della Sala, F. *J. Chem. Theory Comput.* **2011**, *7*, 2439–2451.
- (52) Laricchia, S.; Constantin, L. A.; Fabiano, E.; Della Sala, F. *J. Chem. Theory Comput.* **2014**, *10*, 164–179.
- (53) Kulkarni, V.; Prodan, E.; Nordlander, P. *Nano Lett.* **2013**, *13*, 5873–5879.
- (54) Lynch, D. W.; Hunter, W. R. In *Handbook of Optical Constants of Solids II*; Palik, E. D., Ed.; Academic Press: San Diego, USA, 1991.
- (55) Marder, M. *Condensed Matter Physics*; Wiley: Hoboken, USA, 2010.
- (56) Liebsch, A. *Phys. Rev. B* **1993**, *48*, 11317–11328.
- (57) Bennett, A. J. *Phys. Rev. B* **1970**, *1*, 203–207.
- (58) Chiarello, G.; Formoso, V.; Santaniello, A.; Colavita, E.; Papagno, L. *Phys. Rev. B* **2000**, *62*, 12676–12679.
- (59) Tsuei, K.-D.; Plummer, E. W.; Liebsch, A.; Kempa, K.; Bakshi, P. *Phys. Rev. Lett.* **1990**, *64*, 44–47.
- (60) Rakic, A. D.; Djurišić, A. B.; Elazar, J. M.; Majewski, M. L. *Appl. Opt.* **1998**, *37*, 5271–5283.
- (61) Raza, S.; Yan, W.; Stenger, N.; Wubs, M.; Mortensen, N. A. *Opt. Express* **2013**, *21*, 27344.
- (62) Li, J.-H.; Hayashi, M.; Guo, G.-Y. *Phys. Rev. B* **2013**, *88*, 155437.

- (63) Charlé, K.-P.; Schulze, W.; Winter, B. In *Small Particles and Inorganic Clusters*; Chapon, C., Gillet, M., Henry, C., Eds.; Springer Berlin Heidelberg, 1989; pp 471–475.
- (64) Okamoto, T. In *Near-Field Optics and Surface Plasmon Polaritons*; Kawata, S., Ed.; Topics in Applied Physics; Springer Berlin Heidelberg, 2001; Vol. 81; pp 97–123.
- (65) Vignale, G. *Phys. Rev. B* **2004**, *70*, 201102.
- (66) Mortensen, N. A.; Raza, S.; Wubs, M.; Søndergaard, T.; Bozhevolnyi, S. I. *Nature Commun.* **2014**, *5*, 3809.

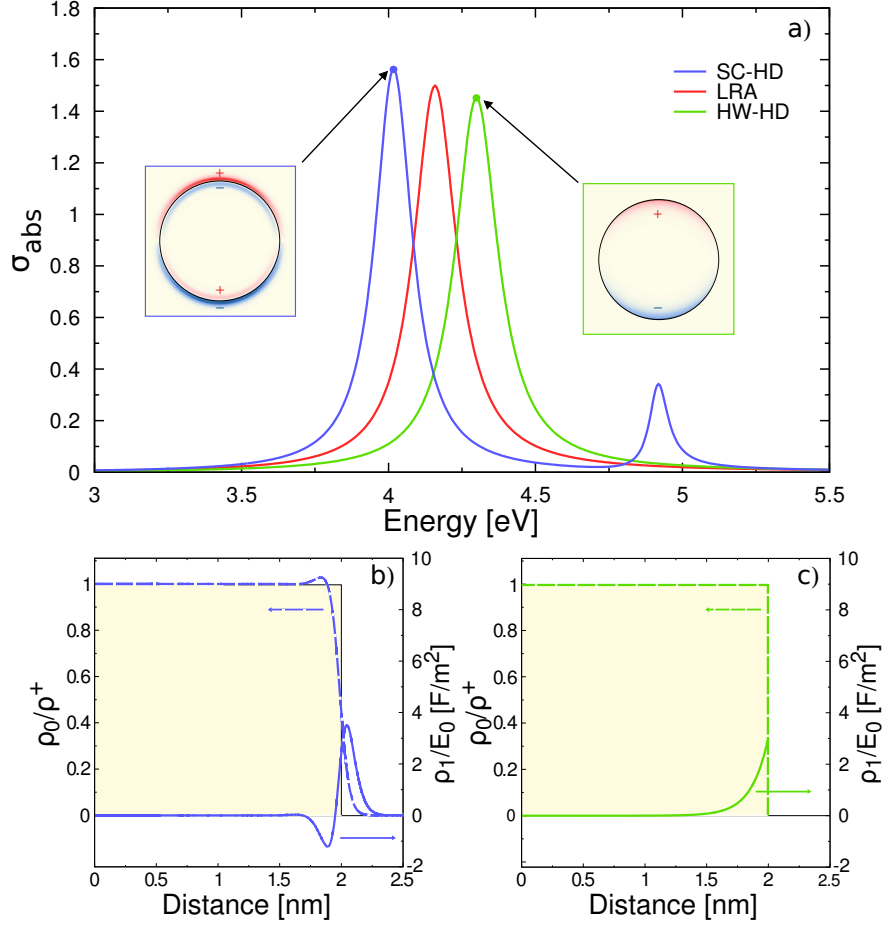


Figure 1: Panel a) Absorption cross section σ_{abs} versus photon energy for a Na cylindrical nanowire of radius $R = 2 \text{ nm}$ in the LRA (red line), the HW-HD model (green line) and the SC-HD model (blue line). The insets show the charge density distributions $\rho_1(\mathbf{r})$ at their respective SPR frequencies for the SC-HD model (blue box) and the HD model (green box). Panel b) SC-HDM model: equilibrium electron charge density ρ_0 normalized to the ion charge density ρ^+ (dashed line), and induced charge density ρ_1 normalized to the perturbing field amplitude E_0 for the SPR, as a function of the distance from the axis of the nanowire. Panel c) As panel b), now for the HW-HD model.

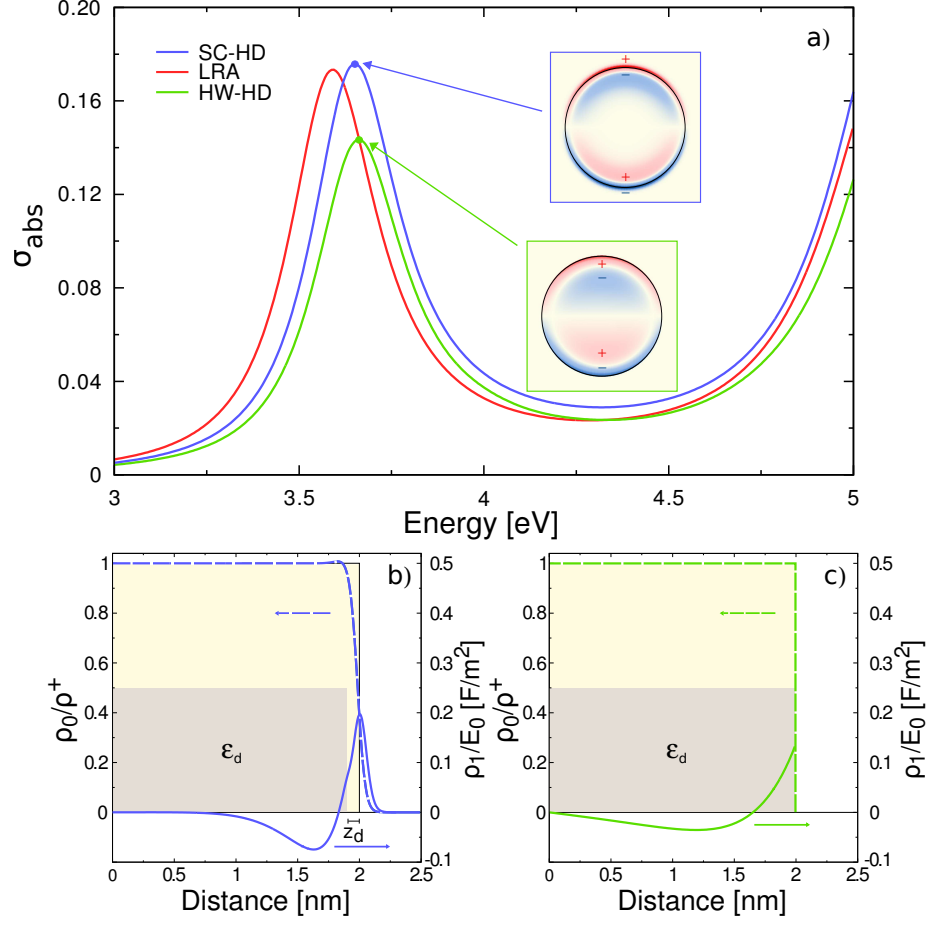


Figure 2: Same as Figure 1, now for Ag nanowires, also with radius $R = 2$ nm.

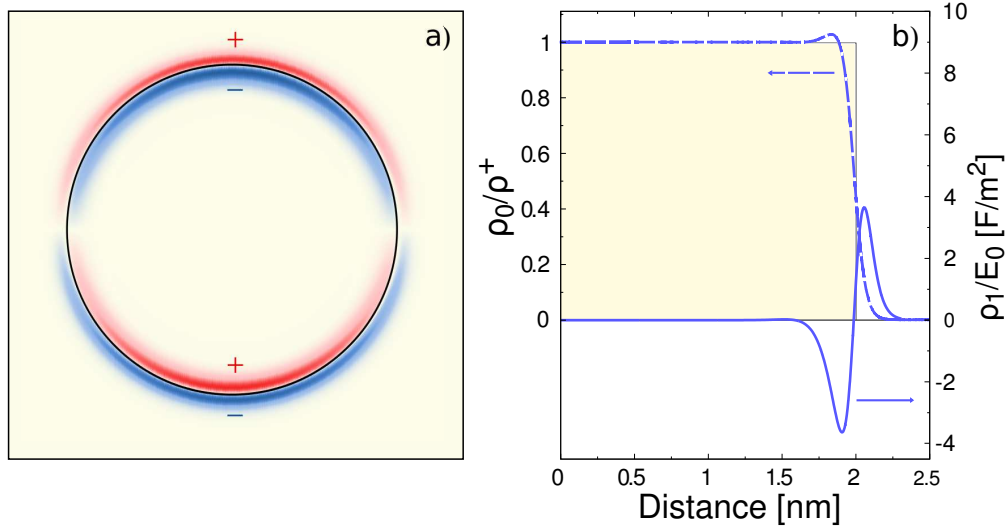


Figure 3: Panel a) Charge density distribution $\rho_1(\mathbf{r})$ for the Bennett resonance for a Na cylindrical nanowire of radius $R = 2$ nm. Same as Figure 1b), now for the Bennett resonance.

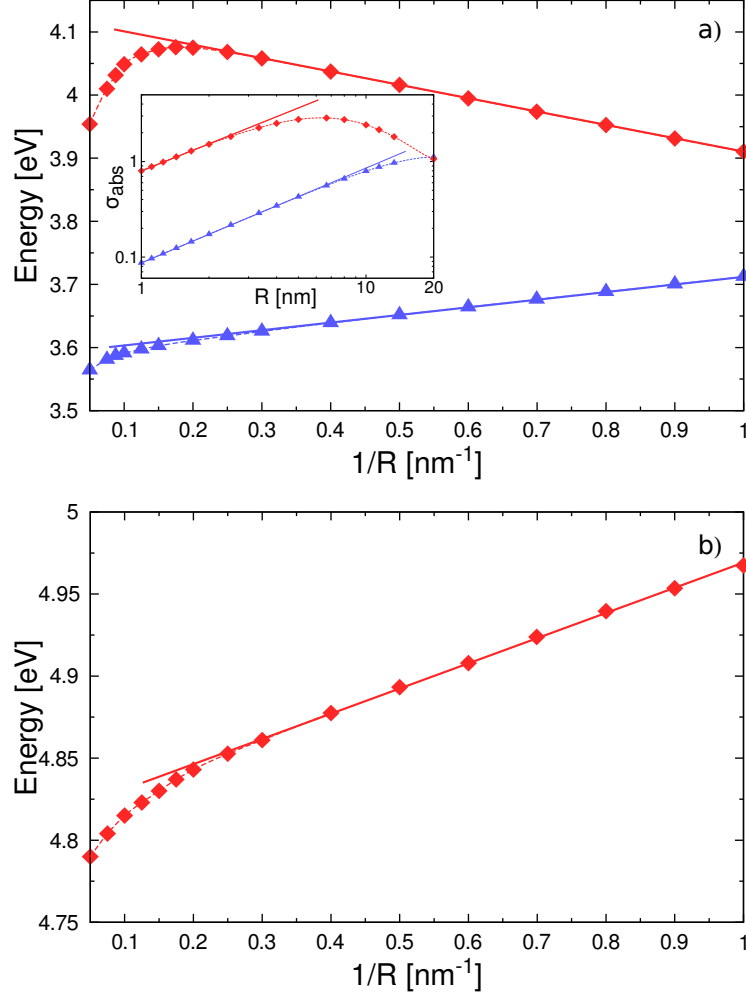


Figure 4: Panel a) Surface plasmon resonance frequency versus the inverse radius $1/R$ for a Na nanowire (red squares) and an Ag nanowire (blue triangles) as calculated in the SC-HD model. The dashed lines are guides to the eye, whereas the full lines illustrate the $1/R$ dependence. Inset: Log-log graphs of the absorption cross section exactly at the SPR versus radius R for a Na nanowire (red squares) and an Ag nanowire (blue triangles) in the LRA model. Panel b) "Bennett" resonance frequency versus the inverse radius $1/R$ for a Na nanowire.